

ScienceDirect



IFAC PapersOnLine 55-37 (2022) 663-668

H_∞ Optimal Control for Maintaining the R2R Peeling Front

C. Martin*, Q. Zhao **, S. Bakshi ***, D. Chen***, W. Li****

The University of Texas at Austin, Austin, TX, 78712, USA

*(cbmartin129@utexas.edu), **(qishenzhao0904@utexas.edu), ***(soovadeep.bakshi@utexas.edu), ****(dmchen@me.utexas.edu), *****(weiwli@austin.utexas.edu)

Abstract: Dry transfer using Roll-to-Roll (R2R) mechanical peeling could significantly increase the throughput and efficiency of the production of 2D materials such as graphene and flexible electronics. Currently, such a R2R process does not exist in industry. For this dry transfer R2R process to be practical for industrial applications, the peeling angle between the growth substrate and the functional material needs to be precisely controlled. In this paper, a nonlinear state space representation of the R2R dry peeling process is formulated with the peeling front velocity variation as a disturbance input. This state space model is used to construct a linear parameter varying (LPV) representation of the system, and a methodology on how to bound the LPV representation within a convex polytopic linear differential inclusion (PLDI) set is presented. This PLDI representation is then used in a linear matrix inequality (LMI) optimization framework to design a full state feedback controller that minimizes the H_{\tilde{\pi}} gain of the connection between the adhesion energy variation and the peeling front geometry. Simulation results demonstrate that this controller improves the precision of the R2R peeling angle, and this increase in precision enables higher web speed. Thus, this technique can be an enabling tool for making R2R mechanical peeling dry transfer of 2D materials a reality in industrial settings.

Copyright © 2022 The Authors. This is an open access article under the CC BY-NC-ND license (https://creativecommons.org/licenses/by-nc-nd/4.0/)

Keywords: Roll-to-Roll (R2R), Polytopic Linear Differential Inclusions (PLDI), Linear Matrix Inequalities (LMI), film peeling, optimal control.

1. INTRODUCTION

Methods have been developed to grow two-dimensional (2D) materials such as graphene (Kobayashi et al., 2013), solar cells (Sondergaard et al., 2012; Krebs et al., 2009), and flexible electronics (Jain et al., 2005) using the roll-to-roll (R2R) methods. R2R processes are superior to batch processes because they are continuous, which allows them to have a higher throughput at higher efficiency. Though there have been R2R process methods proposed for producing devices, there has, until recently, been little information in the literature on how to transfer the devices from the growth substrate in a continuous manner. For graphene, the majority of the proposed R2R production techniques involve using chemical vapor deposition (CVD) to grow the material on a growth substrate such as copper (Kobayashi et al., 2013; Xin et al., 2018). Once this CVD graphene is produced, traditional methods for transferring the material from its growth substrate to a target substrate are discontinuous and involve using hazardous chemical etchants (Zhang et al., 2013). In contrast, the R2R dry transfer approach used in this paper is continuous and does not involve any chemical etchant (Xin et al., 2018; Zhao et al., 2020; Zhao et al., 2021; Hong et al., 2022). Thus, it is environmentally benign and has the potential to have a higher throughput than previous methods.

For an R2R dry transfer process, controlling the peeling angle is critical to a successful transfer. Past works have identified controlling the peeling angle as the critical objective in peeling CVD graphene (Zhao et al., 2020). In addition, researchers (Qin et al., 2015) investigated how peeling angle affected the

quality of peeled silicene—a material that has similar properties as graphene—and they found that the optimum peeling angle was 45°. This finding suggests that there is potentially an optimal peeling angle for graphene, and that a control process that maintains the peeling front at that angle would be critical for R2R dry transfer. For shear-assisted transfer printing of flexible electronics, stamps have been developed whose adhesion energy depends on the angle of retraction and other shear forces (Linghu et al., 2018; Yang et al., 2012; Yoo et al., 2014; Zhou et al., 2019). This dependance on the angle suggests that a R2R transfer printing method could be developed where a change in the peeling angle could be used to control which substrate a printed electronic device adheres to. Another important issue that is endemic to all R2R systems is that the web tensions and velocities are coupled, so it is challenging to maintain acceptable tension precision as the web velocity increases (Abjadi et al., 2008; Xu et al., 2002). In the system studied in this paper, since the peeling angles depend on the web tensions, variation in the peeling angles tends to increase as the web speed increases, so angle error tolerance requirements can be a limiting factor to production line throughput. Therefore, controlling the angles of the peeling front is critical for the effectiveness of R2R dry transfer of graphene, and it has the potential to be the foundation of future work in a R2R transfer process for flexible electronics.

This paper presents the development of an H_{∞} optimal controller to maintain the peeling angles of an R2R peeling system. A nonlinear state-space representation of the system is developed with experimentally calibrated parameters, and this

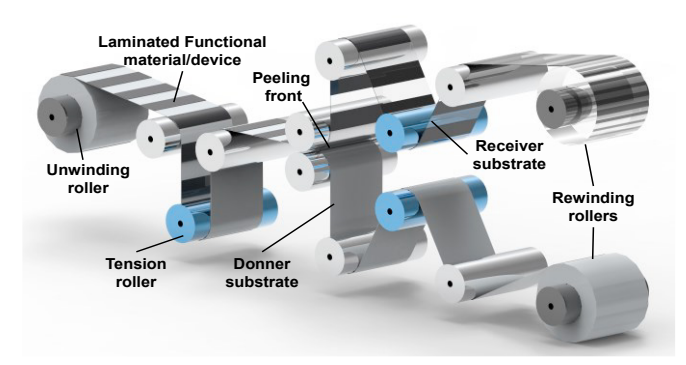


Figure 1. The R2R Peeling System (Zhao et al., 2021). (An illustration of the entire R2R peeling system)

state space representation is reformulated into an LPV framework. A PLDI approached is then used to bound the LPV representation within a convex matrix set. This PLDI representation enables the use of LMI constraints to build an optimal controller, the goal of which is to minimize the H_∞ gain of the connection between the error in the peeling angles and the variation in the adhesion energy. The state space model used to build the PLDI is formulated such that the variation in the peeling front velocity is treated as a disturbance input, and the two peeling angles are explicitly included within the state vector. The control methodology presented in this paper builds on that presented in (Martin et al., 2021) in that this paper uses LMI-constrained optimization to optimize over the entire PLDI set, and the controller in this paper is explicitly designed to improve angle precision. In addition, we demonstrate that this new control strategy allows the R2R peeling system to operate at a higher throughput compared to a typical feedback approach.

An important benefit of the PLDI convexification method used in this paper is that it is reversible, meaning it is possible to maintain a connection between the manufacturing system / process parameters and the control law. This connection allows the engineer to use methods such as control co-design (Garcia-Sanz, 2019) to simultaneously optimize the system parameters and the controller. This advantage does not exist in other convexification methods such as the Koopman operator method (Mezic, 2015; Korda, 2018), where the nonlinear system is linearized in a higher dimensional space with no obvious connection to physical parameters. Thus, the PLDI convexification method is particularly suited for real-world engineering problems with unknowns in both design and control phases, such as the R2R dry transfer process.

The paper begins with the Models and Methods section, which contains the R2R model, the new system representation used for control design, a description of how to build the PLDI, and the process used to find the optimal controller. The next section, Discussions and Results, presents and analyzes simulation results that compare the performance of the H_{∞} optimal controller to the performance of three tuned feedback controllers. The paper ends with concluding thoughts.

2. MODELS AND METHODS

2.1 The R2R peeling model

Modeling of an R2R peeling system, previously developed in (Zhao et al., 2021), is summarized in this section. The system

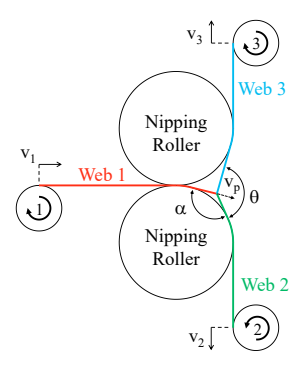


Figure 2. The R2R Peeling Front (Zhao et al., 2021). (An illustration of the peeling front parameters)

is illustrated in Fig. 1, and the process flow is as follows. The functional material or device, laminated to the donor substrate, is unwound from the unwinding roller. It then goes through the nipping rollers, where the functional material is peeled from the donor substrate onto the target substrate. The used donor substrate and the receiver substrate with the functional material are each rewound on separate rewinding rollers. Fig. 2 illustrates the peeling front where the functional material transfers from the donor to the target substrate, and Table 1 defines the symbols that will be used to represent the parameters of the peeling system.

Table 1. Peeling System Parameters

Symbol	Meaning			
α, θ	Peeling angles (radians)			
t_i , $i = 1, 2, 3$	Web tensions (N)			
v_i , i = 1, 2, 3	Web velocity (m/s)			
l_i , $i = 1, 2, 3$	Unstretched length of the web (m)			
ε_i , $i = 1, 2, 3$	Web strain (m/m)			
v_p	Peeling front velocity (m/s)			
G	Energy release rate (N/m)			
Γ	Adhesion Energy (N/m)			
R_i , i = 1, 2, 3	Radius of the roller (m)			
J_i , i = 1, 2, 3	Moment of inertia of the roller (kg-m ²)			
f_i , $i = 1, 2, 3$	Friction coefficient of the roller (m/s)			

The time derivatives of the web velocities and unstretched lengths are defined by the following four equations.

$$\dot{v}_i(t) = -\frac{R_i^2}{J_i}t_i(t) + \frac{R_i}{J_i}u_i(t) - \frac{f_i}{J_i}v_i(t), i = 2,3$$
 (1)

$$\dot{l}_1(t) = \frac{v_1(t) - v_p(t)}{1 + \varepsilon_1(t)} \tag{2}$$

$$\dot{l_2}(t) = \frac{v_p(t)}{1 + \varepsilon_1(t)} - \frac{v_2(t)}{1 + \varepsilon_2(t)}$$
(3)

$$\dot{l}_3(t) = \frac{v_p(t)}{1 + \varepsilon_1(t)} - \frac{v_3(t)}{1 + \varepsilon_3(t)}$$
(4)

Note that the translational velocity of the unwinding roller, v_l , is considered a constant parameter in this study. v_p , the peeling front velocity, is defined as the speed of the separating webs as observed from web 1 at the peeling front.

In addition, the tensions of the three webs can be numerically obtained as a function of the three unstretched web lengths. The energy release rate G can then be determined as a function of those three tension values. G is a significant parameter

because it physically cannot exceed the adhesion energy, Γ , of the two laminated webs.

The primary difficulties in modelling this system revolve around the peeling front velocity, as it is an unknown function of the web tensions, web velocities, and Γ . To address this challenge, a finite difference approach is adapted for the simulations in this study (Zhao et al., 2021). Starting with the web tensions and velocities from the previous timestep, the algorithm first uses equation (1) to find v_2 and v_3 at the current timestep. Next, it assumes that $v_p = 0$ at the previous timestep, and then it uses (2)-(4) and a numerical scheme to find the tensions at the current timestep. Using those tensions, if the energy release rate G is larger than Γ , the algorithm enforces the constraint that $G = \Gamma$, and uses the same numerical scheme to find v_n at the previous timestep and the three tensions at the current timestep. Then, the algorithm repeats these steps. More details on the algorithm can be found in (Zhao et al., 2021). This model has been experimentally validated, and it accurately predicts the behavior of the physical system. However, stability analysis is difficult since the R2R dry transfer system is inherently unstable. This reality motivates feedback control.

2.2 The System Representation Used for Control Design

A control-oriented state-space form of the peeling front model is presented here. To develop the controller, we define the peeling front velocity in the following manner:

$$v_n = v_1 + dv_n \tag{5}$$

where dv_p is a stochastic variable. This representation is justified because it is not possible to represent v_p as solely a function of the state variables, as it also depends on Γ , which varies significantly and unpredictably. Thus, the stochastic nature of Γ is captured in this system representation by representing v_p as a stochastic variable. Using this representation, (2)-(4) can be re-written as:

$$\dot{l}_1(t) = \frac{-dv_p(t)}{1+\varepsilon_1(t)} \tag{6}$$

$$\dot{l}_{2}(t) = \frac{v_{1} + dv_{p}(t)}{1 + \varepsilon_{1}(t)} - \frac{v_{2}(t)}{1 + \varepsilon_{2}(t)}$$
(7)

$$\dot{l}_3(t) = \frac{v_1 + dv_p(t)}{1 + \varepsilon_1(t)} - \frac{v_3(t)}{1 + \varepsilon_3(t)}.$$
 (8)

Next, a connection is drawn between the tension derivatives and the unstretched length derivatives. The three tensions can be found as a function of the three unstretched lengths numerically. The partial derivative of each tension value with respect to each unstretched length can also be found numerically. Using this fact, we define the tension derivatives in the following manner (Martin et al., 2021):

$$\dot{t}_{i} = \frac{\partial t_{i}}{\partial l_{1}}(t) \cdot \dot{l}_{1} + \frac{\partial t_{i}}{\partial l_{2}}(t) \cdot \dot{l}_{2} + \frac{\partial t_{i}}{\partial l_{3}}(t) \cdot \dot{l}_{3}, \ i = 1, 2, 3 \ (9)$$

where the unstretched length derivatives are defined using (6)-(8). Now, using (1) and (9), we define the system in the following state-space form:

$$\dot{x} = f(x, w, u), x = [v_2, v_3, t_1, t_2, t_3]^T, w = dv_p, u = [u_2, u_3]^T$$
(10)

The state-space representation (10) will now enable the construction of the PLDI set and the optimal controller.

2.3 PLDI Convexification

In order to formulate the PLDI representation and the convex LMI-constrained optimal control for the R2R system, first we represent the system in a linear parameter varying (LPV) form. To begin, define the following three variables:

$$A(t) = \frac{\partial f}{\partial x}(t), B_w(t) = \frac{\partial f}{\partial w}(t), B_u = \frac{\partial f}{\partial u}, \tag{11}$$

and notice that B_u is constant here. Using this representation, the system is described in the LPV form:

$$\dot{x} = A(t)x + B_w(t)w + B_u u \tag{12}$$

The goal of the controller presented in this paper is to minimize the effect of variation in the adhesion energy on the peeling angle errors at a certain target operating point. Let that target operating point be \hat{x} , \hat{u} , where \hat{x} is a desired system state and \hat{u} is the constant control output associated with that state. Let \hat{w} be zero. Next, the state vector is transformed so that the peeling angles θ and α are system states. To do this, define the following two functions,

$$\theta = g_{\theta}(t_1, t_2, t_3) = \cos^{-1} \frac{t_1^2 - t_2^2 - t_3^2}{2t_2 t_3}$$
 (13)

$$\alpha = g_{\alpha}(t_1, t_2, t_3) = \cos^{-1} \frac{t_3^2 - t_1^2 - t_2^2}{2t_1 t_2}.$$
 (14)

Then, linearize these two functions about the operating point \hat{x} in the following manner,

$$T_{\theta,\alpha} = \begin{bmatrix} \frac{\partial g_{\theta}}{\partial x} \\ \frac{\partial g_{\alpha}}{\partial x} \end{bmatrix}_{x = \hat{x}} \tag{15}$$

And use it to form the following transformation matrix,

$$T = \begin{bmatrix} I_{3\times3}, 0_{3\times2} \\ T_{\theta,\alpha} \end{bmatrix}. \tag{16}$$

Let the new state vector be $\tilde{x} = [v_2, v_3, t_1, \theta, \alpha]^T \cong Tx$. Thus, the transformed system can be presented in the following LPV representation.

$$\dot{\tilde{x}} = \tilde{A}(t)\tilde{x} + \tilde{B}_{w}(t)w + \tilde{B}_{u}u, \text{ where } \tilde{A}(t) = TA(t)T^{-1}, \\ \tilde{B}_{w}(t) = TB_{w}, \tilde{B}_{u} = TB_{u}$$
(17)

Now that the equilibrium operating point and transformed system have been defined, the LPV system representation (17) will be bounded within a convex, polytopic, matrix set. Using experimental data, one can find the lower and upper bounds on each cell of $\tilde{A}(t)$ and $\tilde{B}_{w}(t)$ in the neighborhood around \hat{x},\hat{u} . These bounds are defined in the following manner,

$$\tilde{A}_{i,j\,min} = \min_{t} \,\tilde{A}(t)_{i,j}, \,\tilde{A}_{i,j\,max} = \max_{t} \,\tilde{A}(t)_{i,j} \qquad (18)$$

$$\tilde{B}_{w_{i min}} = \min_{t} \tilde{B}_{w}(t)_{i}, \tilde{B}_{w_{i max}} = \max_{t} \tilde{B}_{w}(t)_{i}$$
 (19)

where t is the timespan of the experiment or simulation, and the subscript i, j denotes the cell in the ith row and jth column. Using these bounds, a matrix set Ω_{PLDI} can be built such that,

$$\Omega_{PLDI} = \{ \left[\tilde{A}, \tilde{B}_{w}, \tilde{B}_{u} \right] \mid \tilde{A}_{i, j \, min} \leq \tilde{A}_{ij} \leq \tilde{A}_{i, j \, max}, \, \tilde{B}_{w_{i} \, min} \leq \tilde{B}_{w_{i} \, max} \}.$$
(20)

This representation creates a polytope of 2^c matrix vertices, where c is the number of cells in $\tilde{A}(t)$ and $\tilde{B}_w(t)$ that vary significantly. In this paper, if $\tilde{A}_{i,j\,min}$ and $\tilde{A}_{i,j\,max}$ differ by more than 10%, then the cell i, j is considered variable. Otherwise, $\tilde{A}_{i,j} = \text{mean} (\tilde{A}_{i,j\,min}, \tilde{A}_{i,j\,max})$. The same is true for \tilde{B}_{w_i} . In this way, only the cells that vary significantly contribute to the list of vertices, thus minimizing the size of the polytopic representation of the matrix set. According to (Boyd, 1994), if there exists a set Ω such that,

$$\left[\frac{\partial f}{\partial x}\frac{\partial f}{\partial w}\frac{\partial f}{\partial u}\right] \in \Omega \tag{21}$$

around some trajectory \bar{x} , \bar{w} , \bar{u} , for a state-space representation like in (22), then,

$$[\dot{x} - \dot{\bar{x}}] \in \operatorname{Co}(\Omega) \begin{bmatrix} x - \bar{x} \\ w - \bar{w} \\ u - \bar{u} \end{bmatrix}.$$
 (22)

Let $\bar{x} = \hat{x}$, $\bar{u} = \hat{u}$, and $\bar{w} = \hat{w} = 0$; and let $x = \tilde{x}$, w = w, and u = u; then Ω_{PLDI} satisfies (21), and because $\hat{x} = 0$ and $Co(\Omega_{PLDI}) = \Omega_{PLDI}$,

$$\dot{\tilde{x}} \in \Omega_{PLDI} \begin{bmatrix} \tilde{x} - \hat{x} \\ w \\ u - \hat{y} \end{bmatrix} . \tag{23}$$

Thus, using this PLDI representation, the state derivative can be bounded within a convex set at any system state $[\tilde{x}, w, u]^T$.

2.4 Controller Development

Before developing the controller, let the exogenous output, the vector that should be minimized, be defined as follows,

$$z = \begin{bmatrix} Q_{w^{\frac{1}{2}}} \\ 0_{2\times 10} \end{bmatrix} \begin{bmatrix} \tilde{x} - \hat{x} \\ \tilde{x}_I \end{bmatrix} + \begin{bmatrix} 0_{10\times 2} \\ R_{w^{\frac{1}{2}}} \end{bmatrix} (u - \hat{u}), \tag{24}$$

where $Q_w^{\frac{1}{2}}$ and $R_w^{\frac{1}{2}}$ are symmetric user-defined weighting matrices, and \tilde{x}_I is a vector containing the integral errors of the states. The goal of the controller is to minimize γ , the induced L_2 gain of the system, which is equivalent to the H_∞ norm.

Induced L₂ gain / H_∞ norm =
$$\sup_{\|w\|_2 \neq 0} \frac{\|z\|_2}{\|w\|_2} \le \gamma$$
 (25)

To build such a controller, the following convex LMI optimization problem (Boyd, 1994) is solved as,

minimize $\gamma > 0$, such that, for $i = 1, ..., 2^c$,

$$\begin{bmatrix} \left(A_{i}Q + Q{A_{i}}^{T} + B_{u,i}Y + C_{z,i}Q + D_{zu,i}Y \right)^{T} \\ +Y^{T}B_{u,i}^{T} + B_{w,i}B_{w,i}^{T} \\ C_{z,i}Q + D_{zu,i}Y - \gamma^{2}I \end{bmatrix} \leq 0, \quad (26)$$

where
$$A_i = \begin{bmatrix} \tilde{A}_i & 0_{5\times 5} \\ 0_{5\times 5} & I_{5\times 5} \end{bmatrix}$$
, $B_{w,i} = \begin{bmatrix} \tilde{B}_{w,i} \\ 0_{5\times 1} \end{bmatrix}$, and $B_{u,i} = \begin{bmatrix} \tilde{B}_u \\ 0_{5\times 2} \end{bmatrix}$ such that $\begin{bmatrix} \tilde{A}_i, \tilde{B}_{w,i}, \tilde{B}_{u,i} \end{bmatrix}$ is one of the 2^c vertices of Ω_{PLDI} as

defined in (20).
$$C_{z,i} = \begin{bmatrix} Q_w^{\frac{1}{2}} \\ 0_{2\times 10} \end{bmatrix}$$
 and $D_{z,i} = \begin{bmatrix} 0_{10\times 2} \\ R_w^{\frac{1}{2}} \end{bmatrix}$, from (24).

Q > 0 and Y are decision variables. Thus, (26) involves finding Y and Q such that γ is minimized while the 2^c LMI constraints are satisfied, which is equivalent to minimizing the H_{∞} norm of the system over all possible LPV system representations near the desired operating point. This LMI-constrained optimization problem is solved using the MOSEK optimization tool (Mosek ApS, 2021). Since this controller synthesis problem optimizes over a set of system representations it cannot be solved using Riccati equations. This reality emphasizes the importance of the LMI framework. Once this optimization problem is solved, the control law is,

$$u = \hat{u} + K \begin{bmatrix} \hat{x} - \hat{x} \\ \theta_I \\ \alpha_I \end{bmatrix}, \text{ where } K = YQ^{-1}.$$
 (27)

This control law guarantees that (25) holds in the neighborhood where Ω_{PLDI} bounds the system representation. Note that (27) is a full-state-feedback controller. This formulation is necessary as no output feedback controller framework currently exists that can minimize the H_{∞} norm of a system representation bound within a PLDI. Fortunately, full-state-feedback is not an issue in this case since it is possible to measure all five system states directly.

3. DISCUSSION AND RESULTS

To test the developed H∞ optimal controller, a simulation was conducted. The system parameters used were based on the experimental setup described in (Zhao et al., 2020). The simulation was conducted using four different controllers around the same operating point. The first three controllers used were tuned tension feedback controllers, which provided baselines to compare the developed controller against. The feedback controllers were designed to have a fast response time, medium response time, and slow response time, respectively. The fourth controller was the H_∞ optimal controller. We chose to compare the H_∞ optimal controller against feedback controllers because they are similar to the controllers used for R2R processes in industry, and we chose to use feedback controllers with different response times to show that, no matter the goal of the feedback controller, the H∞ optimal controller has superior disturbance rejection performance. The reference state was $\hat{v}_2 = .0045$ m/s, $\hat{v}_3 =$.0045 m/s, $\hat{t}_1 = 10.16$ N, $\hat{\theta} = 124.4$ degrees, and $\hat{\alpha} = 96.5$ degrees, representing a typical operation point for the R2R dry peeling process. The adhesion energy Γ was modeled as a stochastic variable with an expected value of 100 N/m and a variance of 20 (N/m)². The goal of these controllers is to minimize the error in the two angles α and θ while rejecting the disturbance caused by the variation in the adhesion energy, as the variation in Γ is the most significant factor impacting the peeling angles. Figure 3 and Figure 4 show the two simulated peeling angles of the system over time using the four different controllers, while table 2 summarizes the performance of the controllers.

Table 2. Angle Error Comparison

Controller Type	Mean $ \Delta\theta $	Mean $ \Delta \alpha $	Max $ \Delta\theta $	Max $ \Delta \alpha $
feedback fast response	1.9196	1.6254	8.2036	6.7214
feedback med. response	1.6513	1.2459	6.8850	4.9428
feedback slow response	1.6398	1.2826	6.2611	4.0291
H _∞ Optimal	1.3918	0.9031	5.6061	3.4621

Table 2 gives the mean and maximum absolute values of the angle errors associated with each controller, where $\Delta\theta=\theta-\hat{\theta}$, and $\Delta\alpha=\alpha-\hat{\alpha}$. In the table, the controller with the best performance in each column is bolded. Note that the proposed H_{∞} controller outperforms the other three controllers

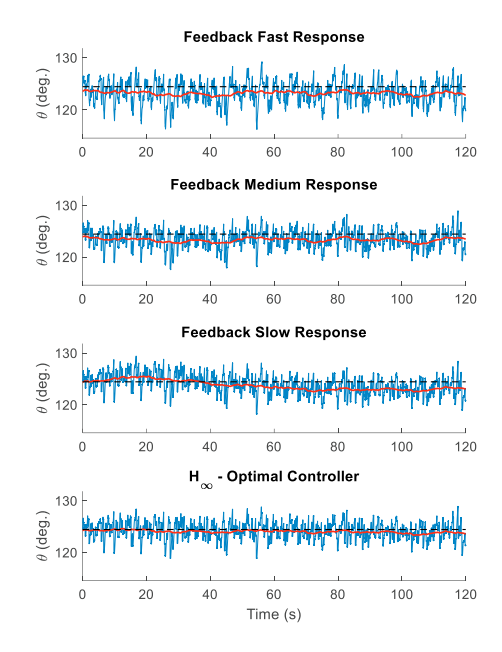


Figure 3. Comparing θ for the four controllers (The thin blue line is $\theta(t)$, the dashed line is $\hat{\theta}$, and the thick red line is a running average of $\theta(t)$)

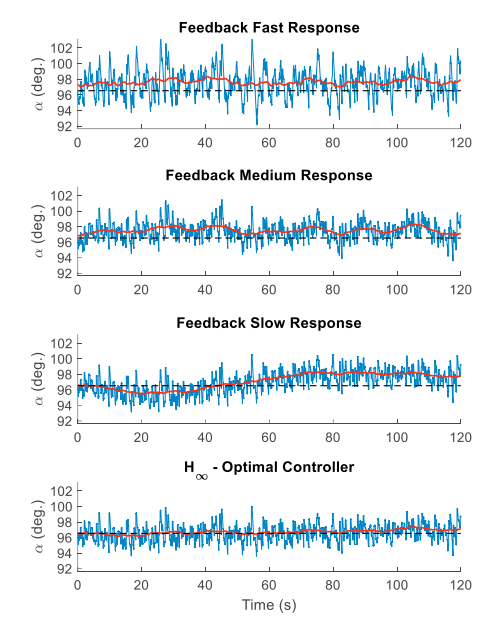


Figure 4. Comparing α for the four controllers (*The thin blue line is* α (*t*), the dashed line is $\hat{\alpha}$, and the thick red line is a running average of α (*t*))

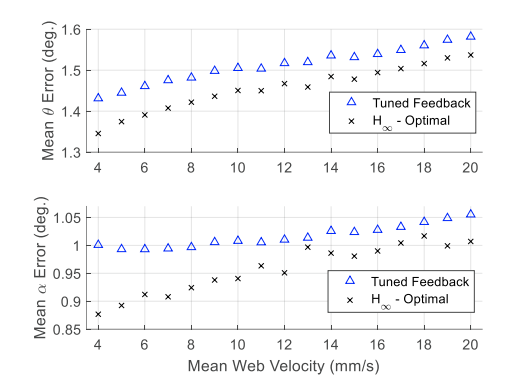


Figure 5. Angle errors at different web velocities (*This figure shows how the simulated mean angle errors change with changing web speed*)

decisively. In addition, the H_{∞} controller has similar or better control effort compared with the other three controllers. Thus, the H_{∞} optimal controller has superior control performance than the three tension feedback controllers.

In addition, by observing the red line in both Fig. 3 and Fig. 4, one can see that the running averages of the two angles stayed closer to the angle set points when the H_{∞} optimal controller was used, which indicates that the steady state error of the H_{∞} optimal controller was smaller than that of the three feedback controllers. The reason for this superior steady state reference tracking is that the proposed controller can respond directly to errors in the two angles and use a model of the system to correct the error. The above results demonstrate that the proposed controller achieves smaller maximum error, mean error, and steady-state error than three well-tuned feedback controllers, and it accomplishes this superior performance with equivalent control effort.

This error minimization enables the web line to move at a higher speed while keeping the angle error below a certain tolerance. Fig. 5 shows the mean angle errors of the simulated R2R system at different web speeds. The figure compares the mean angle errors of the H_{∞} optimal controller with that of a well-tuned feedback controller, analogous to those used to make Figures 3 and 4, that was optimized over the range of velocities studied.

Note that for both the tuned feedback and H_{∞} optimal control schemes, the mean angle errors increase with increasing web speed. However, the angle errors are always smaller using the H_{∞} optimal controller, which enables higher throughput. For example, if there was a design requirement that the mean θ error needed to be kept below 1.5°, then the maximum web processing speed could only be 9 mm/s using the well-tuned feedback controller, while the H_{∞} optimal controller would allow web speeds as high as 16 mm/s, an increase of 78%. Thus, in addition to increasing the angle precision of the peeling process, the H_{∞} optimal control scheme can allow the R2R mechanical peeling system to operate at a higher speed. This success indicates that the proposed controller could be an enabling tool for the R2R dry transfer of 2D materials.

4. CONCLUSIONS

This paper presents the development of an H_{∞} optimal controller for the R2R peeling process. A method to represent

the complex dynamics of the peeling front in state space form is demonstrated, and that novel representation is reformulated into an LPV form. This LPV representation is then bounded within a convex PLDI. A convex optimal control problem is then solved using LMI constraints at each vertex of the PLDI to minimize the H_{∞} norm of the system. This optimal controller is then compared against well-tuned feedback controllers. The proposed controller demonstrates superior peeling angle disturbance precision through effective rejection. Furthermore, this enhanced disturbance rejection also allows the system to operate within a required tolerance at high speeds. For future work we intend to test these results on our experimental testbed. In essence, the proposed control design has the potential to significantly improve the angle precision and increase the production throughput of the R2R peeling system, thus significantly improving the production efficiency of two ground-breaking technological fields: 2D functional materials such as graphene and flexible electronics.

5. ACKNOWLEDGEMENT

This work is based upon work supported primarily by the National Science Foundation under Cooperative Agreement No. EEC-1160494 and CMMI-2041470. Any opinions, findings and conclusions or recommendations expressed in this material are those of the author(s) and do not necessarily reflect the views of the National Science Foundation.

REFERENCES

- Abjadi, Navid R., et al. (2008). Nonlinear Sliding-Mode Control of a Multi-Motors Web Winding System without Tension Sensor. 2008 IEEE International Conference on Industrial Technology.
- Boyd, Stephen (1994). *Linear Matrix Inequalities in System and Control Theory*. Society for Industrial and Applied Mathematics.
- Garcia-Sanz, Mario. (2019). Control Co-Design: An Engineering Game Changer. Advanced Control for Applications: Engineering and Industrial Systems, vol. 1, no. 1.
- Hong, N., et al. (2022). Roll-to-Roll Dry Transfer of Large-Scale Graphene. *Advanced Materials*, vol. 34, no. 3, 210665.
- Jabbar, Kadhim A., and Prabhakar R. Pagilla (2016). Optimal Velocity Profile Design for Transport of Viscoelastic Webs in Roll-to-Roll Manufacturing. 2016 American Control Conference (ACC).
- Jain, K., et al (2005). Flexible Electronics and Displays: High-Resolution, Roll-To-Roll, Projection Lithography and Photoablation Processing Technologies for High-Throughput Production. *Proceedings of the IEEE*, vol. 93, no. 8, pp. 1500–1510.
- Kobayashi, Toshiyuki, et al (2013). Production of a 100-m-Long High-Quality Graphene Transparent Conductive Film by Roll-to-Roll Chemical Vapor Deposition and Transfer Process. *Applied Physics Letters*, vol. 102, no. 2, p. 023112.
- Korda, Milan, and Igor Mezić (2018). Linear Predictors for Nonlinear Dynamical Systems: Koopman Operator Meets Model Predictive Control. *Automatica*, vol. 93, pp. 149–160.

- Krebs, Frederik C., et al (2009). A Roll-to-Roll Process to Flexible Polymer Solar Cells: Model Studies, Manufacture and Operational Stability Studies. *Journal of Materials Chemistry*, vol. 19, no. 30, p. 5442.
- Linghu, Changhong, et al (2018). Transfer Printing Techniques for Flexible and Stretchable Inorganic Electronics. *Npj Flexible Electronics*, vol. 2, no. 1.
- Martin, Christopher, et al (2021). "PLDI-Based Convexification for Roll-to-Roll Dry Transfer Control." Modeling, Estimation, and Control Conference (MECC).
- Mezic, Igor (2015). On Applications of the Spectral Theory of the Koopman Operator in Dynamical Systems and Control Theory. 2015 54th IEEE Conference on Decision and Control (CDC).
- Mosek ApS, (2021). The MOSEK optimization toolbox for MATLAB manual. Version 9.10.
- Qin, Zhao, et al (2015). Peeling Silicene from Model Silver Substrates in Molecular Dynamics Simulations. *Journal* of Applied Mechanics, vol. 82, no. 10.
- Søndergaard, Roar, et al (2012). Roll-to-Roll Fabrication of Polymer Solar Cells. *Materials Today*, vol. 15, no. 1-2, pp. 36–49.
- Xin, Hao, et al (2018). Roll-to-Roll Mechanical Peeling for Dry Transfer of Chemical Vapor Deposition Graphene. *Journal of Micro and Nano-Manufacturing*, vol. 6, no. 3.
- Xin, H. and Li, W., (2018). A review on high throughput roll-to-roll manufacturing of chemical vapor deposition graphene. *Applied Physics Reviews*, vol. 5, no. 3, 031105.
- Xu, Yulin, et al (2002). Adaptive Rejection of Quasi-Periodic Tension Disturbances in the Unwinding of a Non-Circular Roll. *Proceedings of the 2002 American Control Conference (IEEE Cat. No.CH37301)*.
- Yang, Sang Yoon, et al (2012). Elastomer Surfaces with Directionally Dependent Adhesion Strength and Their Use in Transfer Printing with Continuous Roll-to-Roll Applications. *Advanced Materials*, vol. 24, no. 16, pp. 2117–2122.
- Yoo, Byungsuk, et al (2014). Elastomeric Angled Microflaps with Reversible Adhesion for Transfer-Printing Semiconductor Membranes onto Dry Surfaces. *ACS Applied Materials & Interfaces*, vol. 6, no. 21, pp. 19247–19253.
- Zhang, Yi, et al (2013). Review of Chemical Vapor Deposition of Graphene and Related Applications. *Accounts of Chemical Research*, vol. 46, no. 10, pp. 2329–2339.
- Zhao, Qishen, et al (2020). Controlling Peeling Front Geometry in a Roll-to-Roll Thin Film Transfer Process. Proceedings of the ASME 2020 15th International Manufacturing Science and Engineering Conference, September 3, 2020, doi.org/10.1115/MSEC2020-8507.
- Zhao, Q., Hong, N., Chen, D., Li, W (2021). "A Dynamic System Model for Roll-to-Roll Dry Transfer of Two-Dimensional Materials and Printed Electronics." *Journal of Dynamic Systems, Measurement, and Control*, vol. 144, no. 7, 071004.
- Zhou, Honglei, et al (2019). "Transfer Printing and Its Applications in Flexible Electronic Devices." *Nanomaterials*, vol. 9, no. 2, p. 283.